Effect of Cross-Linker Functionality on the Adhesion of Highly Cross-Linked Polymer Networks: A Molecular Dynamics Study of Epoxies

Mesfin Tsige* and Mark J. Stevens

Sandia National Laboratories, P.O. Box 5800, MS 1411, Albuquerque, New Mexico 87185-1411

Received July 9, 2003; Revised Manuscript Received November 5, 2003

ABSTRACT: The effect of cross-linker functionality and interfacial bond density on the fracture behavior of highly cross-linked polymer networks bonded to a solid surface is studied using large-scale molecular dynamics simulations. Three different cross-linker functionalities (f = 3, 4, and 6) are considered. The polymer networks are created between two solid surfaces with the number of bonds to the surfaces varying from zero to full bonding to the network. Stress−strain curves are determined for each system from tensile pull and shear deformations. At full interfacial bond density the failure mode is cohesive. The cohesive failure stress is almost identical for shear and tensile modes. The simulations directly show that cohesive failure occurs when the number of interfacial bonds is greater than in the bulk. Decreasing the number of interfacial bonds results in cohesive to adhesive transition consistent with recent experimental results. The correspondence between the stress−strain curves at different f and the sequence of molecular deformations is obtained. The failure stress decreases with smaller f while failure strain increases with smaller f.

I. Introduction

The adhesion of high strength polymer networks to a solid surface is one of their most important and practical properties.[1,2] Such adhesives present a complex problem for both theory and experiment with basic problems remaining unsolved. Progress has recently been made for adhesives with no strong chemical bonds across the interface such as polymer−polymer interfaces[2,3] and pressure-sensitive adhesives.[4] However, strong adhesives such as epoxies present distinct difficulties which have not yet been overcome. Determining the structure of the polymer network near the interface and determining its connection to the mechanical properties are two basic issues to be resolved for such adhesives. Unfortunately, such detailed measurements are not yet possible. Here we present molecular dynamics (MD) simulations of highly cross-linked polymer networks bonded to a rigid surface. Using MD simulations, we can directly determine the local structure of the adhesive as a function of deformation and simultaneously calculate the stress−strain curves.

Bulk polymer melts and networks have been successfully treated using simple coarse-grained bead−spring models for a while now.[5,6] The development of large-scale molecular dynamics (MD) simulations and the increased computational power has now reached the point where treatment of adhesives is possible.[7−12] Epoxies and highly cross-linked polymer networks present more complex systems to study. We have started from a coarse-grained model to simplify the task as much as possible, yet maintain the essential physical characteristics. Following the success of the initial work,[7,13] we are now ready to study the effects of varying key aspects of the adhesive system in a systematic manner. An important issue is the transition between adhesive and cohesive failure as a function of the interfacial bond density.[14,15] The cross-linker functionality f is a key element of the network structure, and understanding its influence is a fundamental issue. Here we present extension of our previous work to include varying f and cohesive failure.

Epoxy adhesives represent a common structural adhesive with diverse applications.[1] Epoxy thermoset networks are chemically cured networks based on the reaction between a resin (e.g., diglycidyl ether of bisphenol A) and a cross-linker. Fracture experiments on bulk epoxies have shown that the bulk failure mechanism changes from crazes to localized deformation zones as the cross-linker density increases.[16] The bulk network structure has been investigated using neutron scattering.[17,18] The bond strength is strongest in the highly cross-linked limit. Recently, Kent et al.[14,15] have studied failure for a system involving an epoxy adhesive on a silicon wafer. Using a mixture of self-assembled monolayers (SAMs), they systematically vary the number of chemical bonds at the interface. The mixture is a combination of methyl-terminated and bromine- or amine-terminated alkylsiloxanes. The methyl-terminated molecules do not form bonds with the epoxy while the bromine- and amine-terminated ones do form bonds. By varying the composition of the mixture, the number of bonds at the surface can range from zero to fully bonded to the network. At high concentrations of bromine, the failure stress is constant and the failure mode is cohesive. At the lowest concentrations, the failure is adhesive and the failure stress is due only to weak van der Waals interactions. Intermediate to these two regimes is a regime in which the failure stress monotonically increases with increasing bromine concentration to the cohesive failure stress. The failure stress in the cohesive regime does not depend on whether the mode is tensile or shear.

The organization of the paper is as follows: in the next section the bead−spring model and details of the simulation method are presented. In section III, the main results of the simulation are presented. The correspondence between the stress−strain curve and the sequence of molecular deformations for three different cross-linker functionalities is discussed. Then the stress−

10.1021/ma034970t CCC: $27.50
Published on Web 12/30/2003

strain curves for the three different functionalities are presented as a function of the number of interfacial bonds. Discussion of the results with comparison to experimental data is given in section IV. Finally, conclusion are presented in section V.

II. Simulation Method

The basic model of highly cross-linked polymer networks is the same as used in earlier work.[7] The polymer network is treated as a bead−spring system. Beads separated by a distance r interact through the standard 6−12 Lennard-Jones (LJ) potential with a cutoff at $2.5d$[6]

$$U_{\mathrm{LJ}}(r) = 4u_0\left[\left(\frac{d}{r}\right)^{12} - \left(\frac{d}{r}\right)^{6}\right] \qquad (1)$$

where u_0 represents the LJ energy and d represents the size of a bead. The masses of all the beads are taken to be equal and all quantities will be in LJ units. The traditional notations of σ and ϵ for stress and strain, respectively, are used.

The bond potential is the sum of the purely repulsive LJ potential (cutoff at $2^{1/6}d$) and a quartic potential. The quartic potential allows bond breaking and prevents unbroken chains from crossing while preserving force continuity. The quartic potential is

$$U_4(r) = \begin{cases} k_4(y - b_1)(y - b_2)y^2 + U_0 & r < r_c \\ U_0, & r > r_c \end{cases} \qquad (2)$$

where $y = r - \Delta r$ shifts the quartic center from the origin. The potential is smoothly cutoff at r_c. Once a bond separation is larger than r_c, the bond is broken and the bond potential between the pair turned off, preventing the bond from re-forming. The parameters in $U_4(r)$ were determined by fitting it with the quartic component to the bond force with the finite extensible nonlinear (FENE) potential at the first zero and the minimum. This just leaves the maximum bond force as a free variable. The potential parameters are $k_4 = 1434.3u_0/d^4$, $b_1 = -0.7589d$, $b_2 = 0.0$, $\Delta r = 1.5d$, and $U_0 = 67.2234u_0$.

The maximum bond force is $156.7u_0/d$, and the maximum LJ force is $2.4u_0/d$. In the simulations a single bead represents several atoms, and the LJ pair interaction represents multiple van der Waals pair interactions. With even just three atoms per bead,[19] each bead−bead interaction represents nine pair interactions and that gives about 590 for the force ratio. This is within a factor of 2 of the ratios for atomic force fields which is a reasonable approximation for a coarse-grained model.

In the simulation a polymer network is confined between two solid surfaces. Each surface consists of particles forming two (111) planes of an fcc lattice with nearest-neighbor distance 1.204. The (111) direction (z direction) is perpendicular to the surfaces, and the system is periodic in the x and y directions. The surface particles are bound to the lattice sites by a harmonic spring with spring constant $100u_0/d^2$. They do not interact with one another, but they interact with the polymer beads via the same LJ potential of eq 1 and some surface particles bond to the polymer network by eq 2. The simulation is performed at constant temperature T using the Langevin thermostat.[20] The integration time step is 0.005τ, and the damping constants are $1\tau^{-1}$ for the monomers and $5\tau^{-1}$ for the surfaces, where τ is the LJ time unit.

To form the networks, we follow a procedure similar to the highly cross-linked epoxies. Epoxies are chemically cured networks formed from a liquid mixture of a resin (e.g., bisphenol A) and a cross-linker.[21] The distance between cross-linkers is rather short as the molecules are short. In the bead−spring model, we set the number of beads between two cross-linkers to be two.[7]

In epoxies, the liquid mixture of a cross-linker and a resin is cross-linked dynamically. In the simulations, a mixture consisting of two bead and three bead molecules is dynamically cross-linked. The three bead molecule has an f-fold functional cross-linker bead already bonded to a two-bead strand. The number of cross-linkers in the system is set by stoichiometry. The strand beads and cross-linker beads have identical LJ parameters. In this work we vary the functionality of the cross-linker: $f = 3$, 4, and 6. The liquid is equilibrated at temperature $T = 1.1u_0$. The network is dynamically formed during a constant temperature simulation. After equilibrating the liquid mixture, curing then is performed in a two-stage process. In the cure simulations, the criterion for bond formation is that the separation between a cross-linker and a strand end or surface particle is less than $1.3d$. First, cross-linkers are bonded to the surfaces. In our previous studies,[7,13] to promote interfacial failure, only one bond per cross-linker to a surface was allowed. In this study, a cross-linker is allowed to bond as much as it can to a surface. That means it can be bonded to a maximum of two surface particles for $f = 3$ and to a maximum of three surface particles for $f = 4$ and also for $f = 6$ due to geometric constraints. This should make the bonding at the surfaces as strong as in the bulk. In the second stage, the cross-linkers are bonded to strands until at least 95% of all possible bonds are made. Zero load is maintained on the surfaces during the cross-linking, allowing the volume to adjust to the curing. Afterward, the temperature is reduced below the glass transition temperature ($T_g = 0.5u_0$) to $0.3u_0$. The top surface moves under a small load so that the density can increase due to the drop in temperature.

The results presented here are for systems of about 90 000 particles which were placed into a rectangular box of dimensions $L_x \times L_y \times L_z$, where L_z is the separation distance between the surfaces. Earlier work showed that larger systems yield similar data particularly the stress−strain curves.[7] We have the same liquid density of $0.8\sigma^{-3}$ ($56.3d \times 31.3d \times 57.9d$) for all the cases studied before cross-linking. In our simulations the bead size corresponds to about $d \approx 1$ nm based on the size of epoxy constituent molecules. On the basis of this mapping the systems have a height of about 60 nm. Estimates of the plastic zone size at a crack tip in epoxies give values of about 10 μm, which is much larger than our system size and for that matter not feasible for molecular level simulations. The simulations thus treat the region at or near the crack tip, although no crack is initially imposed. Strains and possibly stresses are much larger in this region than the macroscopic measured values.

Both tensile and shear deformations simulations are performed where the surfaces are moved with a uniform velocity. All the results presented here are for surface velocity of $v = 0.01d/\tau$. The velocity dependence was

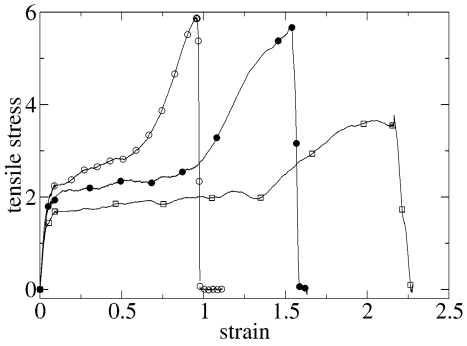

Figure 1. Tensile stress−strain curves for the three different functionalities. The open squares are for $f = 3$, the solid circles are for $f = 4$, and the open circles are for $f = 6$. Stress is in LJ units.

studied in ref 7. For the shear simulations, the surface is pulled in the *x*-direction.

III. Results

A. Effect of Cross-Linker Functionality. Figure 1 shows the stress−strain behavior for tensile pull for three different functionalities: $f = 3$, 4, and 6. A similar form is observed for all the systems. As described in detail in the previous publication,[7] the stress−strain behavior for all the systems is characterized by an initial linear elastic response, followed by yield, followed by a plateau regime, followed by a rise in the stress as bonds are stretched, and finally the system fails. Though the deformation behavior shown here may be general, the height of the peak at the yield point and the failure strain can be sensitive to system size. However, the system size considered in the present study is large enough to avoid the system size effect. We now will describe how the yield stress (σ_y), failure stress (σ_f), and failure strain (ϵ_f) depend on *f*. An extensive discussion of the magnitude of σ_f and its correspondence to measured values is given in ref 7.

The yield stress for all the systems occurs at a yield strain of about 0.1. This strain is related to the maximum in the LJ force to separate neighboring pairs of beads.[7,22] The simulation result shows that the yield stress increases with an increase in the functionality of the cross-linker. This may be due to the fact that after creating the equilibrated network (i.e., just before applying the load), the system with higher functionality was found to be denser (Table 1) though all the systems were cross-linked at the same initial liquid density.

The plateau regime, where the stress is constant for a range of strains, also depends on the functionality of the cross-linker. The plateau occurs because the strands between cross-linkers are being pulled taut while no bond breaking occurs. The plateau regime in Figure 1 has a range of strain of about 0.4 for $f = 6$, 0.9 for $f = 4$, and increases to about 1.3 for $f = 3$. The larger range of the plateau for smaller *f* is a reflection of how the monomers in the strands are packed in the system. For the purposes of this discussion, let "strand" be the four beads of our resin molecule along with a cross-linker at each end. This strand is the fundamental unit of the network to be deformed by the applied strain. The maximum possible strain required to make such a strand taut is 2. This is demonstrated with the help of Figure 2. The most compact state for a strand is a close-packed conformation (part of a triangular lattice). The figure clearly shows that the tensile strain required to deform the close-packed conformation into the linear conformation is either 1.3 or 2. How compact the initial network structure is will determine the strain required to achieve taut strands. To determine this structure, we calculated the radial distribution function for the two cross-linkers in a strand. Figure 3 shows this distribution function g_{XX}, where *X* here stands for cross-linker type, at zero strain. The first peak in g_{XX} is at $r \approx 1.1d$ corresponding to Figure 2a and is largest for $f = 3$ and smallest for $f = 6$. This indicates that the strands in the $f = 3$ case are typically very compact at zero strain with the cross-linkers in a strand being spatial near neighbors. The networks with larger *f* have fewer compact strands and thus require less strain to make the strands taut; therefore, their plateau regions are shorter. Moreover, the largest peak for $f = 6$ is the second peak at $r \approx \sqrt{3}d$. For $f = 6$ this separation represents the average distance between such cross-linkers, implying in this case that cross-linkers are spatial next-nearest neighbors on average corresponding to Figure 2b. Finally, we note that the maximum possible separation between two cross-linkers in a strand is approximately $3d$ for the linear conformation. Since g_{XX} goes to zero before $r = 3d$, no strand is in this linear state at zero strain.

The observed difference in g_{XX} between the different functionalities can be attributed to two different sources. First, because of the stoichiometry, the cross-linker density in our system decreases with increase in *f*. This results in increasing the average distance between cross-linkers as we increase *f*. The second source is the excluded volume around a cross-linker due to the bonded strands. Smaller *f* have less excluded volume, allowing enough free volume for a second cross-linker. It is not surprising that $f = 6$ has a small peak at $r \approx 1.1d$ since the excluded volume in this case is a large fraction of the available volume. Figure 3 implies that as *f* increases the path from one cross-linker to the other at zero strain is longer, i.e., closer to being taut. Thus, less strain is needed for larger *f* to make the cross-linker−cross-linker segments taut, and the plateau regions in the stress−strain curves are shorter.

After the plateau regime the stress rises because some of the strands are now taut and the bonds must stretch on further displacement. In this regime bonds start to break. The slope of the stress−strain curve in this regime increases with *f* because the bond density increases with *f*, resulting in more bonds being stressed. In all cases the bond breaking finally results in complete fracture and drop in stress to zero.

All the three cases shown in Figure 1 fail cohesively as discussed in the next section. The values of tensile strength and strain at failure are given in Table 1 where the failure is taken as the strain at the midpoint between the failure stress (peak) and zero stress after the peak. As *f* decreases, the failure stress decreases while the failure strain increases. It is interesting to note that the difference between the failure stress values of $f = 6$ and $f = 4$ is very small compared to the difference between $f = 4$ and $f = 3$. In general, the work to failure, which is given by the integral of the stress−strain curve, increases with decreasing *f* as shown in Table 1.

Examination of configurations in the tensile simulations just before the system fails shows that $f = 3$ develops voids within the bulk while almost no voids occur at $f > 3$. Figure 4 shows snapshots of $f = 3$ and 4

Table 1. Simulation Results for the Three Different Functionalities *f* at Full Bonding to the Substrate[a]

f	ρ	$\sigma_{f,t}$	$\epsilon_{f,t}$	W_t	$\sigma_{f,s}$	$\epsilon_{f,s}$	W_s	$\epsilon_{\langle P\rangle}$	$\epsilon_{\max P}$
3	0.954	3.6	2.2	5.2	3.5	3.0	5.0	1.7	2.1
4	0.982	5.7	1.6	4.8	5.6	2.2	4.3	1.3	1.5
6	1.004	5.9	1.0	3.1	5.6	1.4	2.8	0.9	1.0

[a] ρ is the density after curing. $\sigma_{f,t}$ and $\epsilon_{f,t}$ are the stress and strain at failure for the tensile mode, respectively, while $\sigma_{f,s}$ and $\epsilon_{f,s}$ are for the shear mode. Also shown are the average strain $\epsilon_{\langle P\rangle}$ and the maximum strain $\epsilon_{\max P}$ required to make the minimal path taut. W_t and W_s are the total work to failure under tensile and shear mode, respectively.

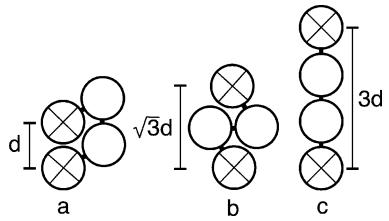

Figure 2. There are two close-packed conformations: (a) one with cross-linker separation of d and (b) one with separation of $\sqrt{3}d$. The fully taut strand (c) has a cross-linker separation of $3d$. Here "strand" includes the two cross-linkers (circle with crosses) as well as the beads between the cross-linkers (circles).

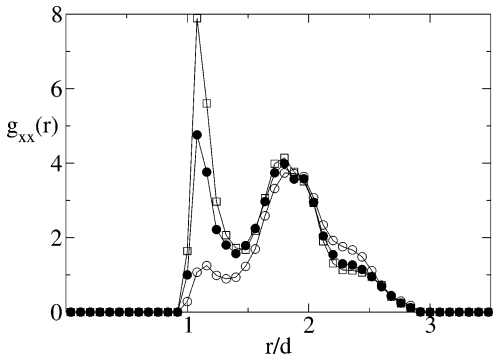

Figure 3. Cross-linker−cross-linker pair correlation function $g(r)$ for the three different functionalities. The open squares are for $f = 3$, the solid circles are for $f = 4$, and the open circles are for $f = 6$.

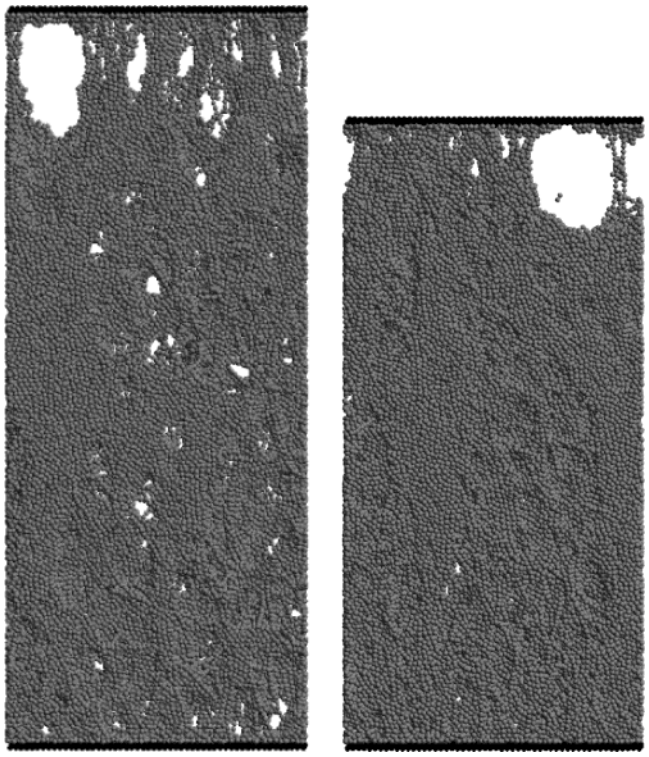

Figure 4. Images before failure under tensile pull for (a) $f = 3$ at $\epsilon = 2.1$ ($\epsilon_f = 2.21$) and (b) $f = 4$ at $\epsilon = 1.5$ ($\epsilon_f = 1.56$). Wall atoms are black and the adhesives are gray.

just before failure. The voids for $f = 3$ case are clearly visible in Figure 4 and have an average volume of about $300d^3$ and are randomly distributed in the bulk. Voids are formed mainly due to the geometry of the network connection within the bulk. Examining the network structure around voids for $f = 3$ shows that the strands are organized in the manner as depicted in the schematic form in Figure 5. For $f > 3$, however, it becomes difficult for the strands to organize in this form since on the average we have more than three strands connected to a given cross-linker. In our simulation these voids became visible at the yield point and found to grow with increase in the deformation of the system.

There is a direct correlation between the failure strains and the network structure.[7] Previously,[7] it has been shown that the average minimal path length of the network can be directly related to the failure strain of the system as described below. For a site on the bottom surface to which the network is bonded, there are many possible paths through the polymer network to the top surface. The shortest path defines the minimal path length P for that particular bottom surface bonding site. There is a set of P for a given system, one for each bonding site at the bottom surface. Using Dijkstra's method,[23] P has been calculated for all bonding sites on the bottom surface and is converted into a strain via the relation $\epsilon_P = (P - L_z)/L_z$, where L_z is the unstrained separation distance between the surfaces. For $\epsilon > \epsilon_P$, some bond within the given minimal path must stretch or break. The simulation shows that $\epsilon_{\langle P\rangle}$, the average of ϵ_P for all the minimal paths, is a fair estimate of the failure strain. In Table 1, $\epsilon_{\langle P\rangle}$ and ϵ_f are compared for the three different functionalities. The average value $\epsilon_{\langle P\rangle}$ is within 10% of ϵ_f for $f = 6$, but that increases to 19% for $f = 4$ and to 22% for $f = 3$. We have observed that as we reduce f the minimal path tends to have a wider distribution. The difference between $\epsilon_{\langle P\rangle}$ and $\epsilon_{\max P}$ becomes significant. Since a system fails by breaking connectivity between the two surfaces, one expects that the failure strain is related to the maximum minimal path. Our simulation shows that $\epsilon_{\max P}$ (Table 1) is in excellent agreement with ϵ_f.

B. Variation of Surface Bond Density. We have pointed out[7] that failure should occur at a plane where the areal bond density is smallest. For the systems considered in Figure 1, cohesive failure occurs. One would then expect that varying the number of bonds across the interface may change the location of failure from cohesive to interfacial. Experimentally, this has been done by coating the surface with a mixture of self-assembled monolayers (SAMs) which allows continuous variation of the number of bondable sites.[14,15] The mixture is a combination of methyl-terminated and bromine- or amine-terminated molecules. The methyl-terminated molecules do not form bonds with the epoxy

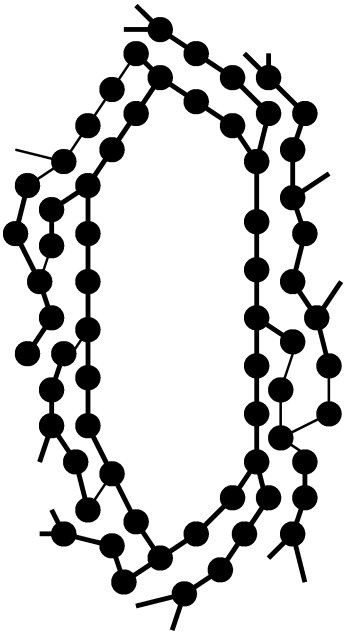

Figure 5. Schematic showing the distributions of strands around a void for $f = 3$.

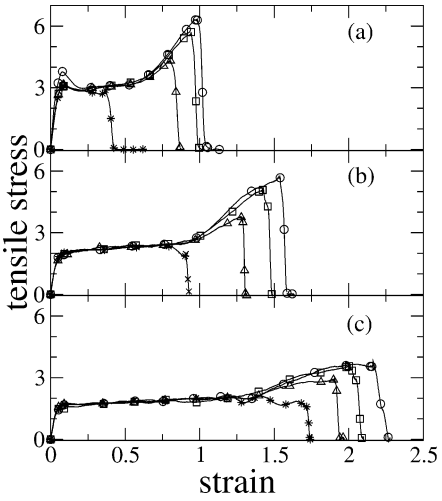

Figure 6. Tensile stress−strain curves for functionalities 6 (a), 4 (b), and 3 (c). The points represent different bondable area fraction C at the bottom surface: 25% (stars), 50% (open triangle), 75% (open square), 100% (open circle).

while the bromine- and amine-terminated ones do form bonds. By varying the composition of the mixture, the number of bonds at the surface can range from 0 to a maximum value. In our simulation, we follow the procedure described earlier[7] and limit the bonding to the solid surface to a fraction of the total area. A set of rectangles on a grid demarcates the nonbonding region on the solid surface. The fractional area of the surface allowed to bond is denoted by C. The fractional number of bonds at coverage C with respect to full coverage is defined as $n_c = N_b(C)/N_b(C = 1)$ which tends to be slightly larger than C since cross-linkers above the edge of a nonbond surface region can move a little and bond to an open site. The limiting values of n_c are 1 and 0, which corresponds to full coverage and no coverage, respectively.

Figure 6 shows the tensile stress−strain curves for the three functionalities as a function of C. The shape of the stress−strain curves is similar for all the systems. The $C = 1$ case represents the typical deformation

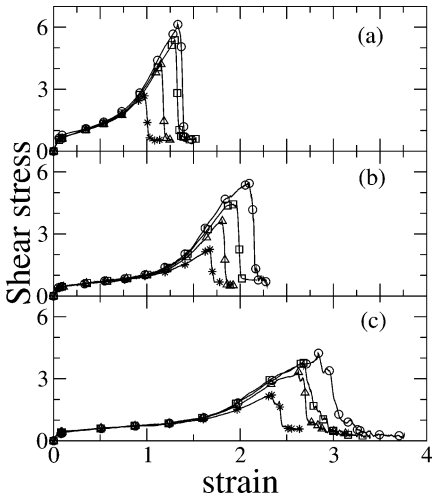

Figure 7. Shear simulation data for functionalities 6 (a), 4 (b), and 3 (c). Points are same as Figure 6.

behavior discussed in section IIIA. The results show that the $C = 1$ stress−strain curve is a master curve for the lower coverage data. At $C < 1$ the stress−strain curves follow that of $C = 1$ until near the failure stress at which point the stress drops to zero. From the plot, we see two types of behavior as a function of coverage. For low coverage ($C \leq 0.25$), where failure occurs without any secondary rise in the stress, the failure stress is primarily determined by the LJ interactions. While bonds are broken at these low coverages, the number of bonds is relatively small with bonds breaking independently. The contribution to stress by a single or a few bonds breaking at a given time is small in comparison with the LJ (i.e., van der Waals) stresses. At high coverage ($C \geq 0.5$), bond stretching makes a significant contribution. Somewhere between $C = 0.25$ and 0.5 the number of bonds being stretched at large ϵ is large enough to be a significant contribution to the stress.

The experiments[14,15] also investigate the behavior of epoxies under mode II (shear) fracture. We thus also performed shear simulations. Figure 7 shows the shear stress−strain curves for the three functionalities as a function of C. Like the tensile case we observe different regions. As found for the tensile mode, the $C = 1$ stress−strain curve is again a master curve and the $C < 1$ curves follow this curve. The deformation sequence is similar to the tensile mode. In this case, the plateau regime has a slow rise in the stress. Comparing Figures 6 and 7 shows that the failure stress in the shear mode is the same as in the tensile mode within the error of the simulations while the yield stress in the shear mode is less than the tensile mode.[7] At sufficiently large ϵ the slope increases as the bonds are being stretched (and broken), since the strands are now taut. Because of geometric factors which can be related to the minimal path,[7] the failure strains for the shear mode are larger than for the tensile mode as shown in Table 1. For $C \geq 0.1$ the failure stress in the shear mode is comparable to the tensile mode.

The transition between cohesive and adhesive failure can be determined from the dependence of the failure stress on C. In Figure 8 we plot the failure stress in both tensile and shear mode as a function of C for $f = 6$. For large values of C near 1 the failure stress is constant, implying cohesive failure. For $0.1 \leq C \leq 0.6$, the failure stress decreases with C which indicates a mixture of cohesive and adhesive failure. For $C < 0.1$

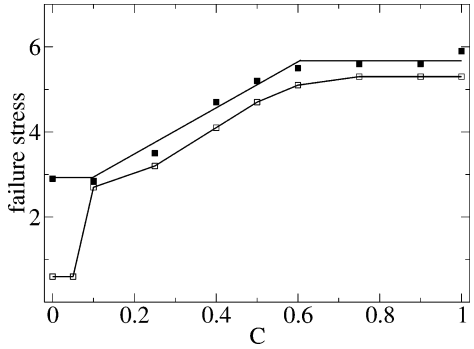

Figure 8. Failure stress in tensile (closed squares) and shear (open squares) simulations as a function of the fractional number of interfacial bonds for the case of $f = 6$.

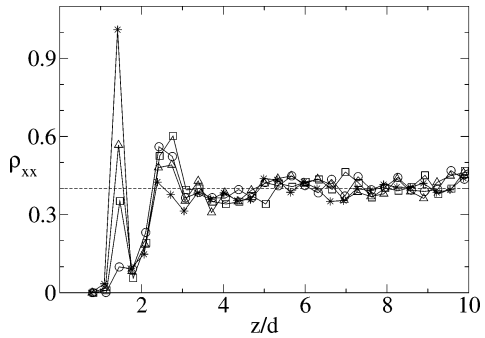

Figure 9. Cross-linker bond density as a function of z for different values of C for the case of $f = 6$. The stars are for $C = 1.0$, the open triangles are for $C = 0.6$, the open squares are for $C = 0.4$, and the open circles are for $C = 0.25$.

we have purely adhesive failure. These three regimes have been observed experimentally by Kent et al.[15]

To examine why the transition from cohesive to adhesive occurs at $C \approx 0.6$ we examine the connectivity of the system as a function of distance from the solid surfaces. Interfacial vs cohesive failure is determined by the location of the broken bonds. Breaking any bond within the segment connecting two nodes is equivalent. Therefore, we examine the connected cross-linker−cross-linker distribution as in Figure 3. We define the location of the cross-linker−cross-linker segment to be the midpoint of the line segment connecting the two cross-linkers. Figure 9 shows the density distribution ρ_{XX} perpendicular to the (bottom) solid wall. The $z = 0$ position corresponds to the position of the inner top surface atoms. We see that for $C = 1$ ρ_{XX} is largest right at the interface. Thus, this plane is the strongest and will not fracture first. Fracture instead occurs at larger z, i.e., bulk. However, we note that the failure occurs near the surface (Figure 10a) and ρ_{XX} appears lower at $z \approx 4d$ than at larger z. As the number of bonds at interface decreases, ρ_{XX} at the interface decreases becoming lower than the bulk. This implies that the location of failure shifts from the bulk to the surface interface as we reduce C. The transition in ρ_{XX} occurs at about $C = 0.6$, the same as in Figure 8 and the same for both tensile and shear mode.

Figure 10 shows images of how the systems fail as we reduce the interfacial bond density. The figure is for $f = 6$ and shows that for $C = 1.0$ (Figure 10a) materials remains at the surface after failure, implying cohesive failure. Reducing the interfacial bond density to $C = 0.25$ (Figure 10b) results in adhesive failure with almost no material on the surface. These images show that while the system fails cohesively the failure is still close

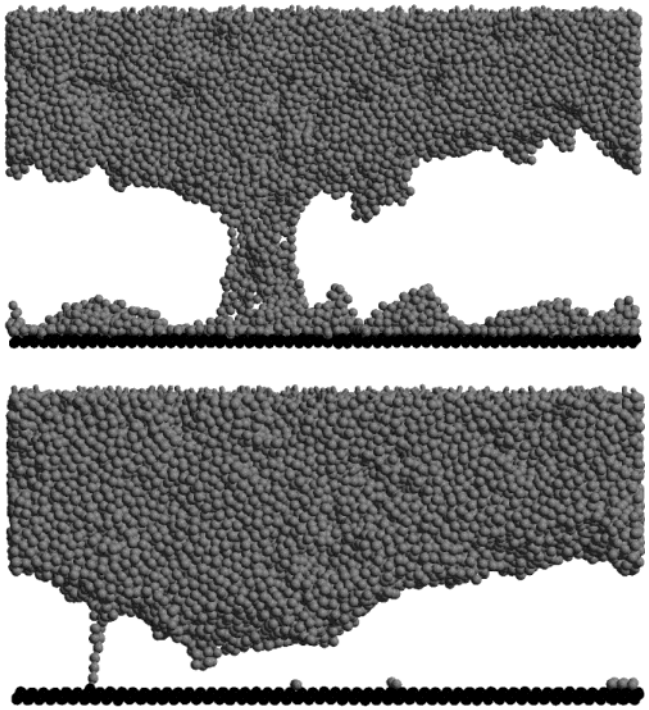

Figure 10. Image of $f = 6$ just before failure for the case of (a) cohesive failure where $C = 1.0$ and $\epsilon = 0.74$ and (b) adhesive failure where $C = 0.25$ and $\epsilon = 0.4$. For clarity, only the bottom part of the systems is shown.

to the interface. For these systems the weakest region does not occur far from the solid surface.

IV. Discussion

Ideally, we would like to compare our results with measurements of the structure of epoxy adhesives near an atomically flat adherent. While such data are not yet available, there are experimental data that control the number of chemical bonds from the epoxy to the substrate.[14,15] As mentioned earlier, the number of interfacial bonds is controlled in these experiments by varying the mixture concentration of SAM molecules with terminal groups that do and do not bond to the epoxy. Comparing Figure 8 with these data yields some striking agreement. Our simulation data exhibit three regimes as do the experiments. At high interfacial bond density there is a cohesive failure regime. At low interfacial bond density there is an adhesive failure regime with the failure stress corresponding only to the van der Waals interactions, i.e., no bonds. In between these two regimes, the failure stress increases monotonically with the number of interfacial bonds.

Another agreement between the simulations and experiments is that the cohesive failure stress is the same for shear and tensile modes. This implies that the failure is not dependent on the macroscopic deformation mode. The simulations show that the condition that determines whether the failure mode is adhesive or cohesive is the bond density in the plane of failure independent of the deformation mode. This simulation result presents a direct link between the adhesive's structure and its strength. This implies that by controlling the network structure there are possibilities for improving adhesive qualities.

In our simulations the cohesive failure occurs close, but not at the interface. This region near the interface is sometimes referred to as the interphase, although it

is not a distinct phase. The presence of the surface can alter the structure of the adhesive near the surface in comparison to the bulk structure. In the model system used here, the liquid mixture before curing has more structure near the surface due to packing effects. This is a well-known phenomena.[24] The liquid and the subsequent cured adhesive are more dense near the surface. This makes the bond density parallel to the surface larger at the surface than in the bulk as we see (Figure 9). However, just a small distance further from the surface and the bond density drops below the bulk value. All the factors that control this effect are not known. However, to pack well, the two bead strands tend to be oriented parallel to the surface in the layers near the surface. Far from the surface, there is no preferred orientation. Apparently, cross-linkers in the layers near the surface tend to bond within their layer as opposed to between layers. Consequently, there is a low bond density between the layers which provides the weak plane for failure.

Our bead−spring model is a minimal model that attempts to capture essential characteristics. By including or changing single aspects of the model, a systematic understanding of the role of these different aspects can be understood. One concern with the present model is that the values of ϵ_f are large due to the flexibility of the model. Typical measured failure strains are much smaller than found in our simulations, but the simulation values of ϵ_f correspond to the local strains at the interface which are larger. Nonetheless, we believe that ϵ_f is larger than would be measured experimentally even on the corresponding length scales (∼50 nm). Since our model is fully flexible (i.e., there is no stiffness in the bead−spring strands), more compact states for the strands are possible. Including molecular stiffness would yield strand structures that at the zero strain would be closer to the fully taut structure; therefore, ϵ_f would be smaller as less strain would be required to make the strand taut and fracture the system. We are presently working on implementing stiffness into our model and will test this expectation. Finally, we note that the failure stress for stiff system may actually increase due to the force needed to bend against the chain stiffness or the angle terms.

The same reasoning as above explains the result that the failure strain is strongly affected by the cross-linker functionality. The failure strain increases because the strands are more floppy and must be strained a greater amount to bring them to the taut state. This is consistent among other measured quantities with the glass transition temperatures being lower for lower f.[25,26] A lower f yields a network with fewer constraints. Thus, a lower temperature is needed for lower f to vitrify the structure. The effect on the work to failure or strength of the network is not so clear, and we believe that multiple aspects of the system influence the strength. For our parameters, we find that the total work to failure is larger for smaller f. It will be interesting to see whether this is still true once molecular stiffness is added to the system.

V. Conclusions

We performed large-scale MD simulations on the mechanical properties of highly cross-linked polymer networks bonded to a solid surface to study the effect of the cross-linker functionality and the number of interfacial bonds on the adhesive to cohesive transition. The networks were made dynamically in a manner similar to epoxy network formation in which the chain length between cross-linkers and the functionality of the cross-linker were controlled. Three different cross-linker functionalities (f = 3, 4, or 6) were studied. The correspondence between the stress−strain curve and the sequence of molecular deformations has been described in detail.

The plateau regime in the stress−strain curve was found to depend on f. Before bonds can be stretched, the strands must be pulled taut. Even for our short strands this requires a rather large strain. The stress is approximately constant during the tightening of the network. The strain range of the plateau regime, which can be related to the density of cross-linker in the system and also to the distribution of beads around it, is found to decrease with an increase in f. Once the strands are taut, further increase in the strain results in an increase in the stress due to bond breaking and finally results in complete fracture and a drop to zero stress. As f increased, failure stress (σ_f) increased while failure strain (ϵ_f) decreased. This is because the bond density is larger at larger f, and thus more bonds are stressed. The overall picture shows that the work to failure decreases with increase in f. The failure strain was found to be directly related to the minimal path through the network from the bottom solid surface to the top surface.

The number of chemical bonds on the solid surface were varied by allowing only some parts of the surface for bonding. When the number of interfacial bonds are greater than any other plane in the bulk, we get cohesive failure. For the systems we studied, increasing the number of interfacial bonds resulted in an adhesive to cohesive transition in agreement with recent experimental observations. For low bond coverage the failure stress was found to be primarily determined by the LJ interactions (corresponding to van der Waals interaction), but at high coverage bond stretching made the dominant contribution.

Acknowledgment. We thank C. Lorenz and M. Kent for many helpful discussions. This work was supported by the DOE under Contract DE-AC04-94AL8500. Sandia is a multiprogram laboratory operated by Sandia Corp., a Lockheed Martin Co., for the DOE.

References and Notes

(1) Kinloch, A. J. *Adhesion and Adhesives*; Chapman and Hall: New York, 1987.
(2) Wool, R. P. *Polymer Interfaces: Structure and Strength*; Hanser Press: New York, 1995.
(3) Creton, C.; Kramer, E. J.; Brown, H. R.; Hui, C. Y. *Adv. Polym. Sci.* **2002**, *156*, 53.
(4) de Crevoisier, G.; Fabre, P.; Leibler, J. C. L. *Science* **1999**, *285*, 1246.
(5) Binder, K., Ed. *Monte Carlo and Molecular Dynamics Simulations in Polymer Science*; Oxford: New York, 1995.
(6) Kremer, K.; Grest, G. *Monte Carlo and Molecular Dynamics Simulations in Polymer Science*; Oxford: New York, 1995; Chapter 4, pp 194−271.
(7) Stevens, M. J. *Macromolecules* **2001**, *34*, 2710.
(8) Baljon, A.; Robbins, M. *Science* **1996**, *271*, 482.
(9) Sides, S. W.; Grest, G. S.; Stevens, M. J. *Phys. Rev. E* **2001**, *64*, 050802.
(10) Sides, S. W.; Grest, G. S.; Stevens, M. J. *Macromolecules* **2002**, *35*, 566.
(11) Baljon, A. R. C.; Robbins, M. O. *Macromolecules* **2001**, *34*, 4200.

(12) Rottler, J.; Robbins, M. O. *J. Adhes. Sci. Technol.* **2003**, *17*, 369.
(13) Stevens, M. J. *Macromolecules* **2001**, *34*, 1411.
(14) Kent, M. S.; Yim, H.; Matheson, A.; Cogdill, C.; Nelson, G.; Reedy, E. D. *J. Adhes.* **2001**, *75*, 267.
(15) Kent, M. S.; Reedy, E. D.; Yim, H.; Matheson, A.; Sorenson, J.; Hall, J.; Schubert, K.; Tallant, D.; Garcia, M.; Ohlhausen, T.; et al. *J. Mater. Res.*, in press.
(16) Glad, M.; Kramer, E. *J. Mater. Sci.* **1991**, *26*, 2273.
(17) Wu, W. L.; Bauer, B. J. *Polymer* **1986**, *27*, 169.
(18) Wu, W. L.; Hunston, D. L.; Yang, H. J.; Stein, R. S. *Macromolecules* **1988**, *21*, 756.
(19) Kremer, K.; Grest, G. S. *J. Chem. Phys.* **1990**, *92*, 5057.
(20) Schneider, J.; Hess, W.; Klein, R. *J. Phys. A* **1985**, *18*, 1221.
(21) Morgan, R.; Kong, F.-M.; Walkup, C. M. *Polymer* **1984**, *25*, 375.
(22) Lorenz, C. D.; Stevens, M. J. *Phys. Rev. E*, in press.
(23) Hu, T. *Combinatorial Algorithms*; Addison-Wesley: Reading, MA, 1982.
(24) Henderson, D., Ed. *Fundamentals of Inhomogeneous Fluids*; Dekker: New York, 1992.
(25) Lesser, A. J.; Crawford, E. *J. Appl. Polym. Sci.* **1997**, *66*, 387.
(26) Crawford, E.; Lesser, A. J. *J. Polym. Sci., Part B* **1998**, *36*, 1371.

MA034970T